Constraining the axion-nucleon coupling and non-Newtonian gravity with a levitated optomechanical device

Lei Chen, Jian Liu, and Ka-Di Zhu*

Key laboratory of Artificial Structures and Quantum Control (Ministry of Education), School of Physics and Astronomy, Shanghai Jiao Tong University, 800 Dong Chuan Road, Shanghai 200240, China

(Received 12 July 2021; accepted 21 September 2022; published 4 November 2022)

In the paper, we propose a scheme to constrain the axion-to-nucleon interaction and non-Newtonian gravity. Here, we consider a levitated optomechanical system consisting of a silica nanosphere and an optical cavity. The total force gradient exerted on this nanosphere modifies its resonance frequency. Based on this, we have developed a quantum optical method to detect and constrain the two exotic forces. Also, we have established prospective constraints on axion-neucleon coupling constants and the Yukawa interaction constant. In addition, these constraints significantly improve the existing bounds.

DOI: 10.1103/PhysRevD.106.095007

I. INTRODUCTION

An axion as a new light pseudoscalar particle was predicted in 1978 [1,2]. Since then, it remains the most compelling solution to the strong-CP problem in QCD and a well-motivated dark matter candidate [3–6]. Because of this, a host of ultrasensitive experiments have been conducted to search for axions and axionlike particles [3,7–11]. Since one main property of the axion is that it can interact with nucleons [7,12], the axion-to-nucleon interaction has been studied by amounts of work (see reviews [13,14]). Consequently, lots of effective constraints [14,15] on the coupling constant g_{an} over a wide axion mass range have been established. Vasilakis *et al.* set constraints at 10^{-4} eV $< m_a <$ 1 μeV via magnetometer measurements [16]. An upper bound most stringent at 1 μeV $< m_a <$ 1.7 meV was derived in Ref. [17] by utilizing the data from a torsion-balance search for Yukawa violations of the gravitational inverse-square law [18]. The strongest constraints at about 1 meV $< m_a <$ 0.5 eV were derived in Ref. [19] from the measurement results of a Casimir-less experiment [20]. Several upper bounds [15,21–25] are derived from measuring some Casimir-effect-based objects including effective Casimir pressure [26,27], the lateral Casimir force between corrugated surfaces [28,29], the difference in Casimir forces [30], the gradient of the Casimir force [31], the Casimir-Polder force [32], and the Casimir force in nanometer separation range [33]. The most stringent constraints at $m_a > 0.5$ eV were obtained from experiments on measuring the forces between protons in the beam of molecular hydrogen [34,35]. The strongest laboratory limits at $m_a > 200$ eV were obtained from the experiment on nuclear magnetic resonance [35]. Though these effective constraints have been established, it is still desirable for us to search for the axion-to-nucleon interaction and set stronger constraints on it.

In this paper, we propose an optomechanical system consisting of a silica nanosphere and an optical cavity which is composed of a mirror and source mass to detect the axion-to-nucleon interaction. In our proposed scheme, the nanosphere is trapped near the surface of the source mass with two separations. Consequently, a difference in the actual resonance frequency of the nanosphere occurs due to the total force gradient exerted on it. Further, this difference can be converted into the distance between two peaks existing in the relevant transmission spectrums. The distance can be both calculated and measured. The disagreement between the computational result and the observation can imply the existence of the exotic interaction. In addition, effective constraints are established for the coupling constants g_{an} and g_{ap} via noise analysis. In the case of $g_{an}^2 = g_{ap}^2$, our constraints on g_{an} improve the existing bounds by several orders of magnitude at about 10^{-4} μeV $< m_a <$ 1 eV.

The "fifth force" hypothesis proposed in 1986 [36] can be considered as a natural outgrowth of many earlier experimental and theoretical studies of non-Newtonian gravity [37]. It also spawned many experiments searching for non-Newtonian gravity. So far, for the purposes of constraining non-Newtonian gravity and testing the gravitational inverse square law at short ranges, many experimental methods have been developed, and various kinds of devices have been used [14,38–42]. However, the non-Newtonian gravity also called the Yukawa interaction can be well constrained only down to the submillimeter range [43], and this gravity at the ultrashort ranges still needs to

*zhukadi@sjtu.edu.cn

be investigated. In this paper, the non-Newtonain gravity is also constrained by the proposed scheme. As a consequence, an upper bound on the interaction constant α is established. This bound improves the most stringent limits by about 2 orders at $\lambda = 10^{-6}$ m.

The remainder of the paper is organized as follows. In Sec. II, we describe the theoretical model. In Sec. III, we demonstrate our detection method. In Sec. IV, we perform the noise analysis and set the prospective constraints. In Sec. V, we summarize the paper.

II. THEORETICAL MODEL

Here, we consider a levitated optomechanical system composed of an optical cavity and a silica nanosphere with $R \sim 10$ nm (see Fig. 1). The length of the cavity is selected as $L = 11$ cm. The right mirror of the cavity, which is made of fused silica and has a thickness of $d \sim 100$ μm, acts as the source mass. According to Ref. [44], a cavity finesse of $\mathcal{F} = 4290$ and a reflectivity of 99.86% of the right mirror can be achieved. The nanosphere is cooled and trapped in the cavity. The power of the trapping laser is selected as $P = 2mw$. In addition, values of several cavity parameters appear in Table I. Applying a pump laser and a probe laser, the Hamiltonian of this system can be written as [45,46]

$$\begin{aligned} H = {} & \hbar\omega_m b^+ b + \hbar\omega_c c^+ c + \hbar g(b^+ + b)c^+ c \\ & + i\hbar E_{\mathrm{pu}}(c^+ e^{-i\omega_{\mathrm{pu}} t} - c e^{i\omega_{\mathrm{pu}} t}) \\ & + i\hbar E_{\mathrm{pr}}(c^+ e^{-i\omega_{\mathrm{pr}} t} - c e^{i\omega_{\mathrm{pr}} t}), \end{aligned} \tag{1}$$

where ω_m is the resonance frequency of the nanosphere resonator and b^+ (b) is the corresponding creation (annihilation) operator; ω_c is the resonant frequency of the cavity and c^+ (c) is the corresponding creation (annihilation) operator; g characterizes the coupling strength between the cavity and the nanosphere; ω_{pu} and ω_{pr} are the frequencies of the pump laser and probe laser, respectively; and E_{pu} and E_{pr} are related to the laser power P by $|E_{\mathrm{pu}}| = \sqrt{2P_{\mathrm{pu}}\kappa/\hbar\omega_{\mathrm{pu}}}$ and $|E_{\mathrm{pr}}| = \sqrt{2P_{\mathrm{pr}}\kappa/\hbar\omega_{\mathrm{pr}}}$, respectively, where κ is the decay rate of the cavity amplitude.

In a rotating frame at a driving field frequency ω_{pu}, the Hamiltonian can be transformed to

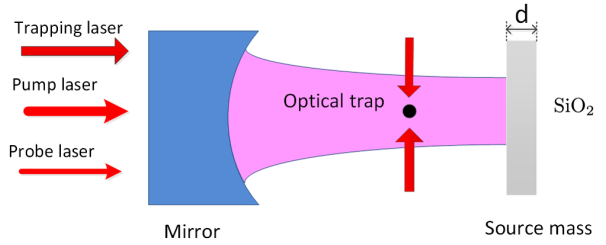

FIG. 1. Schematic setup. A silica nanosphere is trapped in a cavity, one mirror of which acts as the source mass.

$$\begin{aligned} \tilde{H} = {} & \hbar\omega_m b^+ b + \hbar\Delta c^+ c + \hbar g(b^+ + b)c^+ c \\ & + i\hbar E_{\mathrm{pu}}(c^+ - c) + i\hbar E_{\mathrm{pr}}(c^+ e^{-i\delta t} - c e^{i\delta t}), \end{aligned} \tag{2}$$

where $\delta = \omega_{\mathrm{pr}} - \omega_{\mathrm{pu}}$ and $\Delta = \omega_c - \omega_{\mathrm{pu}}$. Defining $\tau \equiv \frac{b+b^+}{\sqrt{2}}$, and applying the Heisenberg equation of motion, we obtain

$$\frac{dc}{dt} = -i\Delta a - ig(b^+ + b)c + E_{\mathrm{pu}} + E_{\mathrm{pr}} e^{-i\delta t}, \tag{3}$$

and

$$\frac{d^2\tau}{dt^2} + \omega_m^2 \tau = -\sqrt{2} g \omega_m c^+ c. \tag{4}$$

Taking the damping terms into consideration, Eqs. (3) and (4) can be rewritten as

$$\frac{dc}{dt} + (i\Delta + \kappa)c = -ig(b^+ + b)c + E_{\mathrm{pu}} + E_{\mathrm{pr}} e^{-i\delta t} \tag{5}$$

and

$$\frac{d^2\tau}{dt^2} + \gamma_m \frac{d\tau}{dt} + \omega_m^2 \tau = -\sqrt{2} g \omega_m c^+ c, \tag{6}$$

where γ_m is the damping rate of the mechanical resonator. Taking expectation values of Eqs. (5) and (6), we obtain

$$\left\langle \frac{dc}{dt} \right\rangle + (i\Delta + \kappa)\langle c \rangle = -ig\sqrt{2}\langle \tau c \rangle + E_{\mathrm{pu}} + E_{\mathrm{pr}} e^{-i\delta t} \tag{7}$$

and

$$\frac{d^2\langle\tau\rangle}{dt^2} + \gamma_m \frac{d\langle\tau\rangle}{dt} + \omega_m^2 \langle\tau\rangle = -\sqrt{2} g \omega_m \langle c^+ c \rangle. \tag{8}$$

We make the ansatz [47] as

$$\langle c(t) \rangle = c_0 + c_+ e^{-i\delta t} + c_- e^{i\delta t}, \tag{9}$$

$$\langle \tau(t) \rangle = \tau_0 + \tau_+ e^{-i\delta t} + \tau_- e^{i\delta t}, \tag{10}$$

where $c_+, c_- \ll c_0$, $\tau_+, \tau_- \ll \tau_0$. Also, we adopt the semiclassical approximation [48,49]:

$$\langle c^+ c \rangle = \langle c^+ \rangle \langle c \rangle \tag{11}$$

and

$$\langle \tau c \rangle = \langle \tau \rangle \langle c \rangle. \tag{12}$$

Substituting Eqs. (9)–(12) into Eqs. (7) and (8), respectively, and neglecting tiny terms, one can finally attain

$$|E_{\mathrm{pu}}|^2 = \left[\kappa^2 + \left(\Delta - \frac{2g^2\sigma}{\omega_m} \right)^2 \right] \sigma, \tag{13}$$

where σ is defined as $\sigma \equiv |c_0|^2$, and

$$c_+ = \frac{E_{\rm pr}K_1(K_1K_2 - iK_4)}{(K_1K_3 - iK_4)(K_1K_2 - iK_4) + K_4^2}, \tag{14}$$

with

$$\begin{aligned} K_1 &= \omega_m^2 - i\delta\gamma_m - \delta^2, \\ K_2 &= -\kappa + i\delta + i\Delta - \frac{2ig^2\sigma}{\omega_m}, \\ K_3 &= \kappa - i\delta + i\Delta - \frac{2ig^2\sigma}{\omega_m}, \\ K_4 &= 2g^2\sigma\omega_m. \end{aligned} \tag{15}$$

To investigate the optical property of the output field for our system, using an input-output relation, which is valid for a one-sided open cavity, $c_{\rm out}(t) = c_{\rm in}(t) - \sqrt{2\kappa}c(t)$, where $c_{\rm in}$ and $c_{\rm out}$ are the input and output operators, respectively, we can obtain the expectation value of the output field as

$$\begin{aligned} \langle c_{\rm out}(t)\rangle = &(E_{\rm pu}/\sqrt{2\kappa} - \sqrt{2\kappa}c_0)e^{-i\omega_{\rm pu}t} \\ &+ (E_{\rm pu}/\sqrt{2\kappa} - \sqrt{2\kappa}c_+)e^{-i(\omega_{\rm pu}+\delta)t} \\ &- \sqrt{2\kappa}c_-e^{-i(\omega_{\rm pu}-\delta)t}. \end{aligned} \tag{16}$$

The transmission of the probe beam, defined as the ratio of the output and input field amplitudes at the probe frequency, is given by [50]

$$t = \frac{E_{\rm pr}/\sqrt{2\kappa} - \sqrt{2\kappa}c_+}{E_{\rm pr}/\sqrt{2\kappa}} = 1 - 2\kappa c_+/E_{\rm pr}. \tag{17}$$

In summary, in this section we describe a levitated optomechanical system and derive the expression of the transmission. Next, we demonstrate our detection method.

III. DETECTION METHOD

Focus on our system. If the nanosphere is trapped near the surface of the source mass, its resonance frequency may be modified by the total force gradient acting on it. Via measuring this modification, we can detect the axion-nucleon interaction and constrain it. In our scheme, the silica nanosphere is trapped with two separations a_0 and a, as shown in Fig. 2. To assure that the resonance frequency of the sphere is not perturbed in the case of a_0, its value is selected as $a_0 \sim 1$ mm. On the other hand, the separation a can be selected as $a \sim 1.6$ μm [51]. And in this case, the resonance frequency may be modified as [31,52,53]

$$\frac{\omega' - \omega_0}{\omega_0} = -\frac{1}{2m_s\omega_0^2}\frac{\partial F_{\rm tot}(a)}{\partial a}, \tag{18}$$

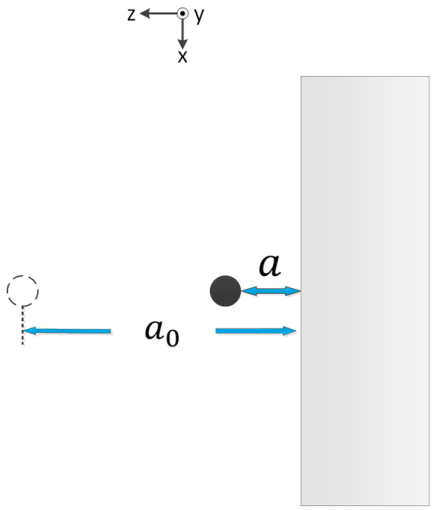

FIG. 2. In our scheme, the silica nanosphere is trapped near the source mass with two separations $a_0 \sim 1$ mm and $a \sim 1.6$ μm, respectively.

where ω_0 is the unperturbed resonance frequency, ω' is the modified one in the presence of the total force $F_{\rm tot}(a)$, and m_s is the mass of the nanosphere. Note that generally $F_{\rm tot}(a)$ is an attractive force which may diminish as the separation increases. From this, we conclude ω' is slightly smaller than ω_0. In the following, we demonstrate how the modification is measured.

First, we choose feasible parameters to investigate the transmission. The unperturbed resonance frequency can be selected as $\omega_0 \sim 1$ kHz [54]. The mechanical quality factor of the nanosphere is selected as $Q \sim 10^8$, which has been achieved in the case of a silica nanoparticle [55]. Thus, the damping rate is calculated as $\gamma_m = \frac{\omega_0}{Q} \sim 10^{-5}$ Hz. The decay rate of the cavity amplitude is chosen as $\kappa = 1$ MHz [56]. For both separations, the parameters used are $\Delta = 0$, $g = 50000$ Hz, $E_{\rm pu} = 1$ kHz, and $E_{\rm pr} = 100$ Hz.

According to Eqs. (14), (15), and (17), one transmission spectrum can be obtained by plotting transmission ($|t|^2$) as the function of δ. Provided that the parameters $(\omega_0, \kappa, \gamma_m, \Delta, g, E_{\rm pr}, E_{\rm pu})$ take values as the above, and substituting ω_m with 1 kHz, $(10^3 + 5)$ Hz, and $(10^3 - 5)$ Hz, respectively, we can obatin three dierent transmission spectrums via plotting as shown in Fig. 3(a). Focus on Fig. 3(a). For the three transmission spectrums plotted with different colors, three resonance peaks, the line widths (full width at half maximum) of which are all 10^{-5} Hz, appear at $(10^3 - 5)$ Hz, 1 kHz, $(10^3 + 5)$ Hz, while the rest of the spectrums coincide with each other. In addition, this line width is designated as Δf in the following. With more numerical analysis, we conclude that the very transmission spectrum at $\omega_0 - 10$ Hz $\le \delta \le \omega_0 + 10$ Hz, plotted with ω_m satisfying $\omega_0 - 10$ Hz $\le \omega_m \le \omega_0 + 10$ Hz and other parameters remaining unchanged, consists of a straight

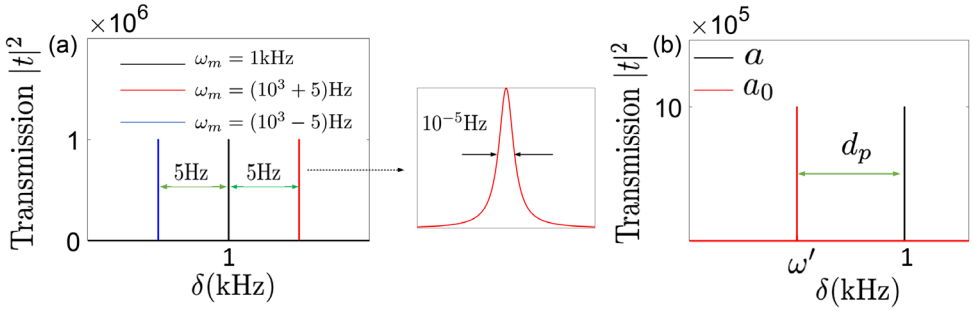

FIG. 3. (a) We plot the transmission ($|t|^2$) as a function of δ when ω_m take different values. The black, red, and blue curves refer to the cases of $\omega_m = 10^3, (10^3+5), (10^3-5)$ Hz, respectively. The parameters used are $\omega_0 \sim 1$ kHz, $\kappa = 1$ MHz, $\gamma_m \sim 10^{-5}$ Hz, $\Delta = 0$, $g = 50000$ Hz, $E_{\mathrm{pu}} = 1$ kHz, and $E_{pr} = 100$ Hz. The middle window is the enlarged red peak with a line width of 10^{-5} Hz. (b) The transmission spectrums corresponding to our scheme. The black peak and the red one correspond to the separations a and a_0, respectively. The distance between two peaks is designated as d_p.

horizontal line with vertical coordinate 0 and a resonance peak at ω_m.

Second, we interpret how the resonance modification is measured. It is assumed that with the help of appropriate adjustment our scheme can be realized experimentally. The corresponding transmission spectrums are shown in Fig. 3(b). The black peak and the red one correspond to the separations a and a_0, respectively. The distance between two peaks is

$$d_p = \omega_0 - \omega'. \tag{19}$$

Then, by measuring d_p, the modification can be determined.

Now, let us draw our attention to the total force $F_{\mathrm{tot}}(a)$ mentioned in the beginning of this section. It can be expressed as [31]

$$F_{\mathrm{tot}}(a) = F_{\mathrm{el}}(a) + F_C(a), \tag{20}$$

where $F_{\mathrm{el}}(a)$ is the electrostatic force and $F_C(a)$ is the Casimir force. For our detection, this electrostatic force should be eliminated. It generally arises from residual potential difference V_0 between the interacting nanosphere and the source mass mirror. This residual potential difference is related to patches and adsorbates on the surfaces of the nanosphere and the mirror. First, the nanosphere in our system has a significant probability to be trapped with a net charge of 0e [57], assuring that the electrostatic force is tiny. Second, provided that a voltage of V is applied to the source mass mirror, the force can be described as [31]

$$F_{\mathrm{el}}(a) = X(V - V_0)^2, \tag{21}$$

where X is a constant. Let $V = V_0$, resulting $F_{el}(a) = 0$.

Then, Eq. (18) can be rewritten as

$$\frac{\omega' - \omega_0}{\omega_0} = -\frac{1}{2m_s\omega_0^2}\frac{\partial F_C(a)}{\partial a}. \tag{22}$$

From Eqs. (19) and (22), we derive

$$d_p = \frac{1}{2m_s\omega_0}\frac{\partial F_C(a)}{\partial a}. \tag{23}$$

The Casimir force here can be considered as the sphere/plate Casimir force, an accurate expression of which can be obtained [58,59]. Thus, the formula describing $F_C(a)$ is attained. Via calculation, we attain that $m_s = 1.05 \times 10^{-20}$ kg. Then, by Eq. (23), we can obtain the value of d_p. Via performing the relating experiment, we can get experimental data about d_p and the relating experimental error. In sum, for d_p, both the calculational result and the experimental one are obtained. After comparing the difference of the two results and the experiment error, whether or not the two results agree with each other within the experimental error is clear. And the disagreement can imply the existence of the exotic interactions. Until now, we have developed a detection method for the exotic interactions. And we establish effective prospective constraints in the following.

IV. PROSPECTIVE CONSTRAINTS

Now, we describe one procedure often used in constraining exotic interactions. First, relevant experiments are performed. Second, the experimental results and the relating theoretical results are compared. If the two are consistent within the experimental errors, there will be no solid evidence for the existence of the hypothetical interactions. In this case, the difference of the two gives us a window where some hypothetical forces may fit. As a consequence of it, effective constraints can be established. In addition, many examples where this procedure has been used can be found in Refs. [13,14,41]. With the help of this procedure,

TABLE I. A summary of cavity parameters.

Cavity length L	Cavity finesse $\mathcal{F}$	Power of trapping laser	Mirror (right) reflectivity	Decay rate of cavity amplitude
11cm	4290	2mW	99.86%	1MHz

prospective constraints on the two exotic interactions are set in the following.

We attempt to estimate the experimental error δd appearing in the relevant experiment at first. In our proposed scheme, while the trapping position of the nanosphere changes, the resonance frequency of it changes simultaneously, and a peak shifts in the transmission spectrum. However, one tiny shift might not be measured due to the noise effect. Generally, there exists a minimum detectable shift $\delta\omega_m$. And it is reasonable to assume $\delta d \sim \delta\omega_m$. Then, the question is to determine the value of $\delta\omega_m$. Here, we use two approaches to resolve this question in the following.

One approach is presented in this paragraph. We derive the fundamental limit imposed by noise. Since nanoparticles levitated in optical fields act as nanoscale oscillators [54], the methods of noise analysis developed in nanomechanical systems [60,61] can be utilized here. In our proposed system, the thermal noise, which originates from thermally driven random motion of the mechanical device, is the dominant noise source. According to Ref. [61], $\delta\omega_m$ can be expressed as

$$\delta\omega_m = \left[\frac{K_B T}{E_C}\frac{\omega_0 \Delta f}{Q}\right]^{1/2}, \tag{24}$$

where $E_C = M_{\text{eff}}\omega_0^2\langle x_c^2\rangle$, M_{eff} is the effective mass of the nanosphere, $\langle x_c\rangle$ is the constant mean square amplitude of it which is driven in a measurement, K_B is Boltzmann's constant, and T is the temperature of the nanosphere. With the relationship $\langle x_c\rangle = \sqrt{K_B T/(M_{\text{eff}}\omega_0^2)}$ [62], we obtain $\delta\omega_m = 10^{-5}$ Hz.

Another approach is demonstrated here. We investigate the minimum detectable shift from an experimental aspect. In the frequency detection regime, the detection limit is closely related to the relevant line width [61,63]. Moreover, Vollmer *et al.* [64] presented an example where the binding of molecules on the surface of a resonator shifts the resonant frequency (see Fig. 8 in Ref. [64]). The demonstration relating to the example (see the caption of this figure) implies that the line width can be assumed as the minimum detectable shift. Thus, we assume $\delta\omega_m = \Delta f = 10^{-5}$ Hz. Now, it is seen that the values of $\delta\omega_m$ obtained from the two approaches are consistent. Then, we assume that $\delta\omega_m = \Delta f$ in the following. With the assumption $\delta d \sim \delta\omega_m$ in the above, we attain that $\delta d \sim \Delta f$.

We assume that if a relating experiment is performed, the measurement of d_p and the value of it obtained by calculation will be consistent within δd. Then, it is attained that

$$\left|\frac{\partial F_e(a)}{\partial a}\frac{1}{2m_s\omega_0}\right| < \delta d, \tag{25}$$

where $F_e(a)$ is the exotic force acting on the nanosphere trapped with the separation a. Since $\delta d \sim \Delta f$ in the above, we can utilize

$$\left|\frac{\partial F_e(a)}{\partial a}\frac{1}{2m_s\omega_0}\right| < \Delta f \tag{26}$$

to set prospective limits.

A. Constraints on axion-nucleon coupling constants

We assume that the exotic force originates from the axion-to-nucleon interaction here. Now, we attempt to derive the expression of the force gradient in Eq. (26). In the system of natural units with $\hbar = c = 1$, the effective potential due to two-axion exchange between two nucleons (protons or neutrons) can be described as [25,65]

$$V(r) = -\frac{g_{ak}^2 g_{al}^2}{32\pi^3 m^2}\frac{m_a}{r^2}K_1(2m_a r), \tag{27}$$

provided that $r \gg 1/m$. Here, g_{ak} and g_{al} are the constants of a pseudoscalar axion-proton $(k, l = p)$ or axion-neutron $(k, l = n)$ interaction, $m = (m_n + m_p)/2$ is the mean of the neutron and proton masses, m_a is the mass of the axion, $K_1(x)$ is the modified Bessel function, and r is the distance between two nucleons. Then, taking into account that the characteristic size of the nanosphere is several orders smaller than the silica mirror, and following Ref. [24], we obtain

$$\frac{\partial F_e(a)}{\partial a} = \frac{\pi}{m^2 m_H^2}C_{\text{Sio}_2}^2 I, \tag{28}$$

with

$$I = \int_1^\infty du\frac{\sqrt{u^2-1}}{u^2}(1-e^{-2m_a u d})e^{-2m_a a u}\Phi(R, m_a u), \tag{29}$$

where the following notation is introduced:

$$\Phi(r, z) = r - \frac{1}{2z} + e^{-2rz}\left(r + \frac{1}{2z}\right). \tag{30}$$

Here, m_H is the mass of the atomic hydrogen, and the coefficient C_{Sio_2} is defined as

$$C_{\mathrm{Sio}_2} = \rho_{\mathrm{Sio}_2}\left(\frac{g_{ap}^2}{4\pi}\frac{Z_{\mathrm{Sio}_2}}{\mu_{\mathrm{Sio}_2}} + \frac{g_{an}^2}{4\pi}\frac{N_{\mathrm{Sio}_2}}{\mu_{\mathrm{Sio}_2}}\right), \tag{31}$$

where ρ_{Sio_2} is the density of the silica; Z_{Sio_2} and N_{Sio_2} are the number of protons and the mean number of neutrons in the molecule Sio_2, respectively; and the quantity μ_{Sio_2} is defined as $\mu_{\mathrm{Sio}_2} = m_{\mathrm{Sio}_2}/m_H$, where m_{Sio_2} is the mean mass of the molecule SiO_2. Note that in Eqs. (27)–(31) the system of natural units is used. Combining Eq. (26) with Eq. (28) and substituting m_s, ω_0, and Δf with the values mentioned above, we obtain

$$\left|\frac{\pi}{m^2 m_H^2} C_{\mathrm{Sio}_2}^2 I\right| < 5.1 \times 10^{-17}(eV)^3, \tag{32}$$

where the system of natural units is used. Using Eqs. (31) and (32), under the conditions of $g_{ap}^2 \gg g_{an}^2$, $g_{an}^2 \gg g_{ap}^2$, and $g_{an}^2 = g_{ap}^2$, respectively, we can derive three inequalities as follows. For $g_{ap}^2 \gg g_{an}^2$, it is

$$\frac{g_{ap}^2}{4\pi} < \frac{m m_H \mu_{\mathrm{Sio}_2}}{\rho_{\mathrm{Sio}_2} Z_{\mathrm{Sio}_2}} \sqrt{\frac{5.1 \times 10^{-17}(eV)^3}{\pi |I|}}. \tag{33}$$

For $g_{an}^2 \gg g_{ap}^2$, it is

$$\frac{g_{an}^2}{4\pi} < \frac{m m_H \mu_{\mathrm{Sio}_2}}{\rho_{\mathrm{Sio}_2} N_{\mathrm{Sio}_2}} \sqrt{\frac{5.1 \times 10^{-17}(eV)^3}{\pi |I|}}. \tag{34}$$

For $g_{an}^2 = g_{ap}^2$, it is

$$\frac{g_{an}^2}{4\pi} < \frac{m m_H \mu_{\mathrm{Sio}_2}}{\rho_{\mathrm{Sio}_2}(Z_{\mathrm{Sio}_2} + N_{\mathrm{Sio}_2})} \sqrt{\frac{5.1 \times 10^{-17}(eV)^3}{\pi |I|}}. \tag{35}$$

The values of several parameters in these equations can be found in Ref. [25]:

$$\frac{Z_{\mathrm{Sio}_2}}{\mu_{\mathrm{Sio}_2}} = 0.503205, \qquad \frac{N_{\mathrm{Sio}_2}}{\mu_{\mathrm{Sio}_2}} = 0.505179. \tag{36}$$

Also, the density of silica in natural units is calculated as

$$\rho_{\mathrm{Sio}_2} = 8.3 \times 10^{-5}\ (\mathrm{MeV})^4. \tag{37}$$

And the values of m and m_H are obtained:

$$\begin{aligned} m &= 938.9150\ \mathrm{MeV}, \\ m_H &= 938.771\ \mathrm{MeV}. \end{aligned} \tag{38}$$

Based on Eqs. (33)–(35), via appropriate substitution (the values of d, a, and R should be in natural units) and calculation, we establish three upper bounds corresponding to each of the three conditions (see Fig. 4). The bound

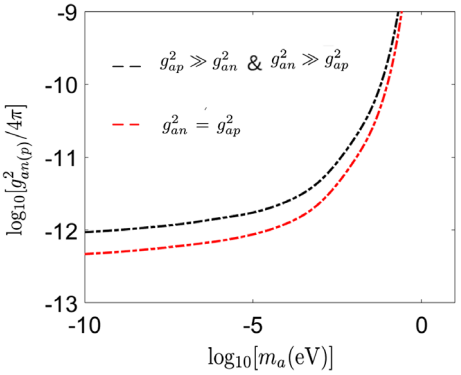

FIG. 4. Constraints on the constant of axion-proton (neutron) interaction as functions of the axion mass m_a. The black curve represents the constraints under the conditions of both $g_{ap}^2 \gg g_{an}^2$ and $g_{an}^2 \gg g_{ap}^2$, while the red one represents the constraints under $g_{an}^2 = g_{ap}^2$.

under $g_{ap}^2 \gg g_{an}^2$ and the one under $g_{an}^2 \gg g_{ap}^2$ are almost the same. Accordingly, both of them are represented by the black curve. And the bound under the most reasonable condition $g_{an}^2 = g_{ap}^2$ [65] is represented by the red curve. In Fig. 5, this bound is compared with existing strongest laboratory constraints on axionlike particles. The upper limit at $m_a < 1$ μeV was obtained with a magnetometer [16] (line labeled "m"). The constraints most stringent at 1 $\mu\mathrm{eV} < m_a < 1.7$ meV were established in Ref. [17] by utilizing the data from the search for violations of the gravitational inverse-square law [18] (line labeled "gr"). The upper limit at about 1 $\mathrm{meV} < m_a < 0.5$ eV was derived in Ref. [19] from the measurement results of the Casimir-less experiment [20] (line labeled "Ca"). The most stringent constraints at $m_a > 0.5$ eV were obtained from experiments on measuring the forces between protons in

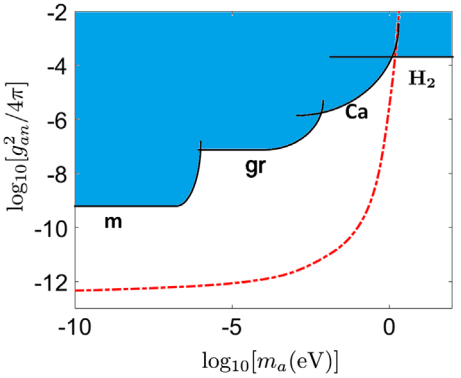

FIG. 5. Constraints on the constant of axion-neutron interaction under the condition $g_{an}^2 = g_{ap}^2$ from the measurement of changes in the precession frequency [16] (line "m"), from the search for violations of the gravitational inverse-square law [17,18] (line "gr"), from a Casimir-less experiment [19,20] (line "Ca"), from measuring the forces between protons [34,35] (line "H_2"), and from our work (dashed red curve). The blue region is excluded.

the beam of molecular hydrogen [34,35] (line labeled "H_2"). The blue region is the excluded parameter space. As can be seen, our constraints significantly improve the upper limit in the wide mass range approximately from 10^{-4} μeV to 1 eV.

B. Constraints on hypothetical Yukawa interactions

Here, we assume that the exotic force $F_e(a)$ in Eq. (26) arises due to the hypothetical interactions. In the short range, the gravitational potential between two masses m_1 and m_2 separated by distance r can be modified as Yukawa potential

$$V_{Yu}(r) = -G_N \frac{m_1 m_2}{r}(1 + \alpha e^{-r/\lambda}), \tag{39}$$

where G_N is the Newtonian gravitational constant, α is the strength of any new interaction, $\lambda = \hbar/m_b c$ is the interaction range, and m_b is the mass of the exchanged boson. By Ref. [66], we attain

$$F_e(a) = -2\pi G m_s \rho_{\mathrm{Sio_2}} \alpha\lambda e^{-\frac{a}{\lambda}}\left(1 - e^{-\frac{d}{\lambda}}\right). \tag{40}$$

Note that here $\rho_{\mathrm{Sio_2}}$ is not in natural units. Substituting Eq. (40) into Eq. (26), we obtain

$$|\alpha| < \frac{\omega_0 \Delta f}{\pi G \rho_{\mathrm{Sio_2}} e^{-\frac{a}{\lambda}}(1 - e^{-\frac{d}{\lambda}})}. \tag{41}$$

Using this equation, we set an upper bound on $|\alpha|$, shown as the dashed red curve in Fig. 6. For comparison, several other upper bounds are plotted in the figure. Line 1 was established by detecting a microsphere response to the hypothetical interactions [67]. Line 2 was established by differential force measurements between a test mass and rotating source masses [20]. Line 3 was obtained via torsion-balance experiments [18]. The green region is the excluded parameter space. It is seen that our bound is most stringent at about 10^{-7} m $< \lambda < 10^{-5}$ m. In addition, our work improves the previous bound (line 1) by several orders. In the work for this bound [67], an optically levitated mass was also used.

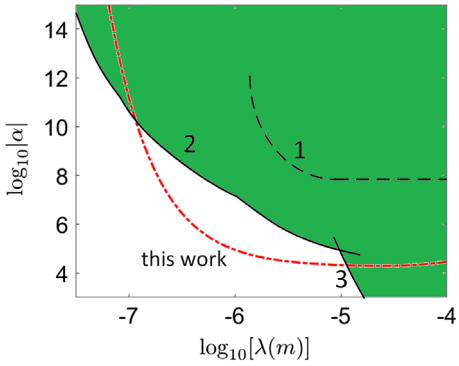

FIG. 6. Limit curve in the $\alpha - \lambda$ parameter space. Constraints were established via an optically levitated microsphere [68] (line 1), differential force measurements [20] (line 2), and torsion-balance experiments [18] (line 3). The dashed red curve represents our work. The green region is excluded.

V. CONCLUSION AND DISCUSSION

In sum, an optical method is developed to constrain the axion-to-neucleon interaction and non-Newtonian gravity. Via the theory of quantum optics, the formula of transmission is obtained. Further, with the help of numerical analysis, how the effect of the total force gradient is reflected on the transmission spectrum is demonstrated. By noise analysis, effective constraints on these two hypothetical interactions are established. In addition, our constraints on the two significantly improve the previous results. Recently, Moore *et al.* described a variety of searches for new physics beyond the standard model of particle physics, which may be enabled in the coming years by the use of optically levitated masses in high vacuum in Ref. [69]. Further, the search of non-Newtonian gravity using an optically levitated microsphere has been realized [67]. Finally, we expect our work to be able to contribute to the search for new physics with levitated masses and be realized experimentally in the near future.

ACKNOWLEDGMENTS

This work is supported by National Natural Science Foundation of China (Grants No. 11274230 and No. 11574206) and Natural Science Foundation of Shanghai (Grant No. 20ZR1429900).

[1] S. Weinberg, A New Light Boson?, Phys. Rev. Lett. **40**, 223 (1978).
[2] F. Wilczek, Problem of Strong p and t Invariance in the Presence of Instantons, Phys. Rev. Lett. **40**, 279 (1978).
[3] P. W. Graham, I. G. Irastorza, S. K. Lamoreaux, A. Lindner, and K. A. van Bibber, Experimental searches for the axion and axion-like particles, Annu. Rev. Nucl. Part. Sci. **65**, 485 (2015).
[4] J. Beringer, J. F. Arguin, R. M. Barnett, K. Copic, O. Dahl, D. E. Groom, C. J. Lin, J. Lys, H. Murayama, C. G. Wohl, W. M. Yao, P. A. Zyla, C. Amsler, M. Antonelli, D. M. Asner, H. Baer, H. R. Band, T. Basaglia, C. W. Bauer, and

J. J. Beatty (Particle Data Group), Review of particle physics, Phys. Rev. D **86**, 010001 (2012).
[5] M. Tanabashi, K. Hagiwara, K. Hikasa, K. Nakamura, Y. Sumino, F. Takahashi, J. Tanaka, K. Agashe, G. Aielli, C. Amsler, M. Antonelli, D. M. Asner, H. Baer, S. Banerjee, R. M. Barnett, T. Basaglia, C. W. Bauer, and J. J. Beatty (Particle Data Group), Review of particle physics, Phys. Rev. D **98**, 030001 (2018).
[6] M. Kawasaki and K. Nakayama, Axions: Theory and cosmological role, Annu. Rev. Nucl. Part. Sci. **63**, 69 (2013).
[7] I. G. Irastorza and R. Javier, New experimental approaches in the search for axion-like particles, Prog. Part. Nucl. Phys. **102**, 89 (2018).
[8] F. Ficek and D. Budker, Constraining exotic interactions, Ann. Phys. (Berlin) **531**, 1800273 (2019).
[9] M. S. Safronova, D. Budker, D. Demille, D. Kimball, A. Derevianko, and C. W. Clark, Search for new physics with atoms and molecules, Rev. Mod. Phys. **90**, 025008 (2018).
[10] L. J. Rosenberg and K. A. van Bibber, Searches for invisible axions, Phys. Rep. **325**, 1 (2000).
[11] T. Braine, R. Cervantes, N. Crisosto, N. Du, and K. W. Murch, Extended Search for the Invisible Axion with the Axion Dark Matter Experiment, Phys. Rev. Lett. **124**, 101303 (2020).
[12] P. Sikivie, Invisible axion search methods, Rev. Mod. Phys. **93**, 015004 (2021).
[13] G. L. Klimchitskaya, Recent breakthrough and outlook in constraining the non-newtonian gravity and axion-like particles from casimir physics, Eur. Phys. J. C **77**, 315 (2017).
[14] V. M. Mostepanenko and G. L. Klimchitskaya, The state of the art in constraining axion-to-nucleon coupling and non-newtonian gravity from laboratory experiments, Universe **6**, 147 (2020).
[15] G. L. Klimchitskaya, P. Kuusk, and V. M. Mostepanenko, Constraints on non-newtonian gravity and axionlike particles from measuring the casimir force in nanometer separation range, Phys. Rev. D **101**, 056013 (2020).
[16] G. Vasilakis, J. M. Brown, T. W. Kornack, and M. V. Romalis, Limits on New Long Range Nuclear Spin-Dependent Forces Set with a K – ^{3}He Comagnetometer, Phys. Rev. Lett. **103**, 261801 (2009).
[17] E. G. Adelberger, B. R. Heckel, S. Hoedl, C. D. Hoyle, D. J. Kapner, and A. Upadhye, Particle Physics Implications of a Recent Test of the Gravitational Inverse Square Law, Phys. Rev. Lett. **98**, 131104 (2007).
[18] D. J. Kapner, T. S. Cook, E. G. Adelberger, J. H. Gundlach, B. R. Heckel, C. D. Hoyle, and H. E. Swanson, Tests of the Gravitational Inverse-Square Law Below the Dark-Energy Length Scale, Phys. Rev. Lett. **98**, 021101 (2007).
[19] G. L. Klimchitskaya and V. M. Mostepanenko, Improved constraints on the coupling constants of axion-like particles to nucleons from recent casimir-less experiment, Eur. Phys. J. C **75**, 164 (2015).
[20] Y. J. Chen, W. K. Tham, D. E. Krause, D. López, E. Fischbach, and R. S. Decca, Stronger Limits on Hypothetical Yukawa Interactions in the 30–8000 nm Range, Phys. Rev. Lett. **116**, 221102 (2016).
[21] V. B. Bezerra, G. L. Klimchitskaya, V. M. Mostepanenko, and C. Romero, Constraining axion-nucleon coupling constants from measurements of effective casimir pressure by means of micromachined oscillator, Eur. Phys. J. C **74**, 2859 (2014).
[22] V. B. Bezerra, G. L. Klimchitskaya, V. M. Mostepanenko, and C. Romero, Constraints on axion-nucleon coupling constants from measuring the casimir force between corrugated surfaces, Phys. Rev. D **90**, 055013 (2014).
[23] G. L. Klimchitskaya and V. M. Mostepanenko, Constraints on axion-like particles and non-newtonian gravity from measuring the difference of casimir forces, Phys. Rev. D **95**, 123013 (2017).
[24] V. B. Bezerra, G. Klimchitskaya, V. Mostepanenko, and C. Romero, Stronger constraints on an axion from measuring the casimir interaction by means of a dynamic atomic force microscope, Phys. Rev. D **89**, 075002 (2014).
[25] V. Bezerra, G. Klimchitskaya, V. Mostepanenko, and C. Romero, Constraints on the parameters of an axion from measurements of the thermal casimir-polder force, Phys. Rev. D **89**, 035010 (2014).
[26] R. S. Decca, D. López, E. Fischbach, G. L. Klimchitskaya, D. E. Krause, and V. M. Mostepanenko, Tests of new physics from precise measurements of the casimir pressure between two gold-coated plates, Phys. Rev. D **75**, 077101 (2007).
[27] R. S. Decca, D. López, E. Fischbach, G. L. Klimchitskaya, D. E. Krause, and V. M. Mostepanenko, Novel constraints on light elementary particles and extra-dimensional physics from the casimir effect, Eur. Phys. J. C **51**, 963 (2007).
[28] H. C. Chiu, G. L. Klimchitskaya, V. N. Marachevsky, V. M. Mostepanenko, and U. Mohideen, Demonstration of the asymmetric lateral casimir force between corrugated surfaces in the nonadditive regime, Phys. Rev. B **80**, 121402(R) (2009).
[29] H. C. Chiu, G. L. Klimchitskaya, V. N. Marachevsky, V. M. Mostepanenko, and U. Mohideen, Lateral casimir force between sinusoidally corrugated surfaces: Asymmetric profiles, deviations from the proximity force approximation and comparison with exact theory, Phys. Rev. B **81**, 115417 (2010).
[30] G. Bimonte, D. López, and R. S. Decca, Isoelectronic determination of the thermal casimir force, Phys. Rev. B **93**, 184434 (2016).
[31] C. Chang, A. A. Banishev, R. Castillo-Garza, G. L. Klimchitskaya, V. Mostepanenko, and U. Mohideen, Gradient of the casimir force between au surfaces of a sphere and a plate measured using an atomic force microscope in a frequency-shift technique, Phys. Rev. B **85**, 165443 (2012).
[32] J. M. Obrecht, R. J. Wild, M. Antezza, L. P. Pitaevskii, S. Stringari, and E. A. Cornell, Measurement of the Temperature Dependence of the Casimir-Polder Force, Phys. Rev. Lett. **98**, 063201 (2007).
[33] M. Sedighi, V. B. Svetovoy, and G. Palasantzas, Casimir force measurements from silicon carbide surfaces, Phys. Rev. B **93**, 085434 (2016).
[34] N. F. Ramsey, The tensor force between two protons at long range, Physica (Amsterdam) **96A**, 285 (1979).
[35] M. P. Ledbetter, M. V. Romalis, and D. Kimball, Constraints on Short-Range Spin-Dependent Interactions from Scalar Spin-Spin Coupling in Deuterated Molecular Hydrogen, Phys. Rev. Lett. **110**, 040402 (2013).

[36] E. Fischbach, D. Sudarsky, A. Szafer, C. Talmadge, and S. H. Aronson, Reanalysis of the Eö tv ös Experiment, Phys. Rev. Lett. **56**, 3 (1986).
[37] E. Fischbach and C. Talmadge, Six years of the fifth force, Nature (London) **356**, 207 (1992).
[38] E. Adelberger, B. Heckel, and A. Nelson, Tests of the gravitational inverse-square law, Annu. Rev. Nucl. Part. Sci. **53**, 77 (2003).
[39] R. D. Newman, E. C. Berg, and P. E. Boynton, Tests of the gravitational inverse square law at short ranges, Space Sci. Rev. **148**, 175 (2009).
[40] J. Murata and S. Tanaka, A review of short-range gravity experiments in the lhc era, Classical Quantum Gravity **32**, 033001 (2015).
[41] G. L. Klimchitskaya and V. M. Mostepanenko, Dark matter axions, non-newtonian gravity and constraints on them from recent measurements of the casimir force in the micrometer separation range, Universe **7**, 343 (2021).
[42] G. L. Klimchitskaya, V. M. Mostepanenko, R. I. Sedmik, and H. Abele, Prospects for searching thermal effects, non-newtonian gravity and axion-like particles: Cannex test of the quantum vacuum, Symmetry **11**, 407 (2019).
[43] W.-H. Tan, A.-B. Du, W.-C. Dong, S.-Q. Yang, C.-G. Shao, S.-G. Guan, Q.-L. Wang, B.-F. Zhan, P.-S. Luo, L.-C. Tu, and J. Luo, Improvement for Testing the Gravitational Inverse-Square Law at the Submillimeter Range, Phys. Rev. Lett. **124**, 051301 (2020).
[44] E. Capocasa, Y. Guo, M. Eisenmann, Y. Zhao, A. Tomura, K. Arai, Y. Aso, M. Marchiò, L. Pinard, P. Prat *et al.*, Measurement of optical losses in a high-finesse 300 m filter cavity for broadband quantum noise reduction in gravitational-wave detectors, Phys. Rev. D **98**, 022010 (2018).
[45] C. Genes, D. Vitali, P. Tombesi, S. Gigan, and M. Aspelmeyer, Ground-state cooling of a micromechanical oscillator: Comparing cold damping and cavity-assisted cooling schemes, Phys. Rev. A **77**, 033804 (2008).
[46] V. Giovannetti and D. Vitali, Phase-noise measurement in a cavity with a movable mirror undergoing quantum brownian motion, Phys. Rev. A **63**, 023812 (2001).
[47] B. R. Masters and R. W. Boyd, *Nonlinear Optics*, 3rd ed. (Academic Press, New York, 2009), p. 315.
[48] Z. Ficek and M. R. Wahiddin, *Quantum Optics for Beginners* (CRC Press, Singapore, 2014).
[49] W. P. Bowen and G. J. Milburn, *Quantum Optomechanics* (CRC Press, Boca Raton, 2015).
[50] S. Weis, R. Riviere, S. Deleglise, E. Gavartin, O. Arcizet, A. Schliesser, and T. Kippenberg, Optomechanically induced transparency, Science **330**, 1520 (2010).
[51] A. Kawasaki, A. Fieguth, N. Priel, C. P. Blakemore, D. Martin, and G. Gratta, High sensitivity, levitated microsphere apparatus for short-distance force measurements, Rev. Sci. Instrum. **91**, 083201 (2020).
[52] M. Liu, J. Xu, G. L. Klimchitskaya, V. M. Mostepanenko, and U. Mohideen, Precision measurements of the gradient of the casimir force between ultra clean metallic surfaces at larger separations, Phys. Rev. A **100**, 052511 (2019).
[53] F. J. Giessibl, Advances in atomic force microscopy, Rev. Mod. Phys. **75**, 949 (2003).
[54] J. Millen, T. S. Monteiro, R. Pettit, and A. N. Vamivakas, Optomechanics with levitated particles, Rep. Prog. Phys. **83**, 026401 (2020).
[55] J. Gieseler, L. Novotny, and R. Quidant, Thermal nonlinearities in a nanomechanical oscillator, Nat. Phys. **9**, 806 (2013).
[56] S. Gröblacher, K. Hammerer, M. R. Vanner, and M. Aspelmeyer, Observation of strong coupling between a micromechanical resonator and an optical cavity field, Nature (London) **460**, 724 (2009).
[57] M. Frimmer, K. Luszcz, S. Ferreiro, V. Jain, E. Hebestreit, and L. Novotny, Controlling the net charge on a nanoparticle optically levitated in vacuum, Phys. Rev. A **95**, 061801 (2017).
[58] A. Bulgac, P. Magierski, and A. Wirzba, Scalar casimir effect between dirichlet spheres or a plate and a sphere, Phys. Rev. D **73**, 025007 (2006).
[59] G. Bimonte, T. Emig, R. L. Jaffe, and M. Kardar, Casimir forces beyond the proximity approximation, Europhys. Lett. **97**, 50001 (2012).
[60] A. N. Cleland and M. L. Roukes, Noise processes in nanomechanical resonators, J. Appl. Phys. **92**, 2758 (2002).
[61] K. L. Ekinci, Y. Yang, and M. L. Roukes, Ultimate limits to inertial mass sensing based upon nanoelectromechanical systems, J. Appl. Phys. **95**, 2682 (2004).
[62] T. Li, S. Kheifets, and M. G. Raizen, Millikelvin cooling of an optically trapped microsphere in vacuum, Nat. Phys. **7**, 527 (2011).
[63] M. Goryachev, B. Mcallister, and M. E. Tobar, Probing dark universe with exceptional points, Phys. Dark Universe **23**, 100244 (2019).
[64] F. Vollmer and L. Yang, Review label-free detection with high-q microcavities: A review of biosensing mechanisms for integrated devices, Nanophotonics **1**, 267 (2012).
[65] E. G. Adelberger, E. Fischbach, D. E. Krause, and R. D. Newman, Constraining the couplings of massive pseudoscalars using gravity and optical experiments, Phys. Rev. D **68**, 062002 (2003).
[66] R. Decca, E. Fischbach, G. Klimchitskaya, D. Krause, D. López, and V. Mostepanenko, Application of the proximity force approximation to gravitational and Yukawa-type forces, Phys. Rev. D **79**, 124021 (2009).
[67] C. P. Blakemore, A. Fieguth, A. Kawasaki, N. Priel, D. Martin, A. D. Rider, Q. Wang, and G. Gratta, Search for non-newtonian interactions at micrometer scale with a levitated test mass, Phys. Rev. D **104**, L061101 (2021).
[68] Y. Kamiya, K. Itagaki, M. Tani, G. Kim, and S. Komamiya, Constraints on New Gravitylike Forces in the Nanometer Range, Phys. Rev. Lett. **114**, 161101 (2015).
[69] D. C. Moore and A. A. Geraci, Searching for new physics using optically levitated sensors, Quantum Sci. Technol. **6**, 014008 (2021).